# A CFD/DEM Approach to Determination of Tortuosity Through Packed Bed of Crushed Rock Particle

Howard Piwang
JE Hoffmann, AB Sebitosi
Stellenbosch University
Email address for correspondence: piwangh@gmail.com

Centre for Renewable and Sustainable Energy Studies

**Abstract**
Packed beds of crushed rock particles are employed in solar thermal power plans as thermal energy storage systems. To model crushed rocks with irregular shapes is tedious; therefore, ellipsoids are used to approximate the shape of the crushed rocks. Discrete element modelling (DEM) is used to generate packed beds using the representative ellipsoids particles. The flow through the voids between the particles is simulated with computational fluid dynamics (CFD). However, the CFD simulations underestimate the flow resistance across a packed bed. The paper introduced tortuosity in an effort to reduce the deviation of pressure drop between real and simulated packed beds. The path lines data for flow velocity across the bed were extracted. The average length of the flow path lines divided by the bed length occupied by particles approximates tortuosity. The tortuosity predicted by the CFD model was validated with a diffusion experiment set up through a packed bed.

*Keywords*: Thermal Storage; Packed bed; Tortuosity; DEM/DEM.

## 1. Introduction

Sub-Saharan Africa is endowed with good solar irradiations with South Africa having one of the best solar resources in the world (Fluri, 2009) making solar power the cheapest option to meet Africa's power needs. Solar thermal power generation has become of interest and with large-scale deployment of this technology, (thermal) energy storage is imperative to mitigate the intermittency of the sun.
Several thermal storage alternatives have been researched mostly on the application of the of solid particles for thermal storage. The materials for use in thermal storage applications should be cheap and readily available (Allen, von Backström and Kröger, 2014) this saves on the total cost of the thermal storage system; (Allen, 2014) experimented on rocks' performance in thermal storage applications at temperatures of 500 – 600 °C. He estimated that the cost of rock bed storage for a solarized Brayton cycle was slightly cheaper than a molten salt thermal energy storage system. The Stellenbosch UNiversity Solar POwer Thermodynamic (SUNSPOT) is a combined solar power that uses the Brayton cycle gas turbine. The central receiver heats up the air to 800°C or more than the compressed air flow through to the gas turbine driving the generators to produce electricity. At night-time, the air is pumped across the bed to extract heat from the rock bed to meet the electricity demand during peak hours. SUNSPOT anticipates the use packed bed of rocks and overuse of molten salts because of the rock availability and cost, but incomplete heat transfer through the bed and pressure drop does impair the economic benefit to the thermal storage and the cycle efficiency of the system.
The use of rocks for thermal storage helps reduce the Levelized Cost of Electricity since the materials are readily available and cheap, able to withstand temperatures of 500-600℃ without cracking (Allen *et al.*, 2014).

Packed beds have particles with varying particle shape, and orientation, shape(Allen, von Backström and Kröger, 2013) found that the pressure drop of packed beds depends significantly on the particle shape, size distribution, packing arrangement and roughness.

(Allen, 2014) confirmed that randomly packed irregular-shaped particles increased the frictional factor by 80%.

(Hölzer and Sommerfeld, 2008) suggests a simple correlation for the drag coefficient of irregular particles that depends on shape and particle orientation. (Du Plessis and Woudberg, 2008a) derived pressure drop in the uniformly sized spherical granules using a representative cell approach. The study adopted varying empirical coefficients from the Ergun equation by investigating the coefficient dependence on the porosity of the particles. (Hoffmann, 2018) suggests that the drag coefficient of irregular particles is expressed in terms of characteristic particle dimension and shape factor. Yet, sphericity cannot account for the influence of particle orientation on pressure drop.

With the advance in computational power, pore-scale models have been developed since modelling for irregular shapes of crushed rocks is time-consuming, (Bagheri *et al.*, 2015) estimate the equivalent diameter of the irregular particles to be equal to the projected surface area of the ellipsoid. This reduces the uncertainty of characterizing irregular particle shapes and sizes.

Several works adopt the use of ellipsoid shapes to determine drag coefficients by using the ellipsoid shapes to approximate crushed rocks. (Hoffmann, 2021) modelled for packed beds consisting of ellipsoid particles. The simulation used an ellipsoid particle with a similar volume and aspect ratio as an average crushed rock. The paper builds on the recommendations from (Hoffmann, 2018). Both papers use ellipsoids to capture anisotropy in the flow field in porous media, but all tend to under-predict the pressure drop.

A study by (Hoffmann, 2021) explored the understanding of the directional effect of the flow resistance across packed beds of ellipsoids to predict the pressure drop, but under-predicted the pressure drop by 27% across the bed of crushed rock particles. The papers limitation was the constant numerical values of coefficients of the resistance tensor. This study contributes to further exploration of the definition of the tortuosity tensor in ellipsoid particle shapes to be introduced to the coefficients to improve on prediction of crushed rocks to experimental data.

The concept of tortuosity was first introduced by (Kozeny, 1927) based on the capillary tube model, and later (Carman, 1937) adjusted the numerical constant empirically for better agreement with experimental results which became famous as the modified Kozeny-Carman's equation. (Ghanbarian *et al.*, 2013) suggests a lack of clear understanding of tortuosity is lacking and yet different experiments and models have been developed, (Duda, Koza and Matyka, 2011) volume integral method, (Garrouch, Ali and Qasem, 2001) diffusion and electric method. The diffusion experiment is one of the most widely adopted methods and (Delgado, 2006) proposed an inexpensive and simple method to determine tortuosity using diffusion through packed beds. The diffusion method is able to predict and understand pore size changes. However, the experimental approach takes a long time or may require specialized equipment. The challenges of correlating experimental diffusion tortuosity to complex geometries restricts the use of experiments (Sun, Tang and Cheng, 2013) thus leading to the adoption of DEM to generate the packed bed and the CFD to solve the fluid flow problems.
This work will introduce tortuosity to improve on the correlation and reduce on the deviation in the works of (Hoffmann, 2021) in the crushed rocks particles by deriving the tortuosity tensor of flow through rock bed using DEM/CFD approach, investigate how to extract local tortuosity from the CFD model, and carry out a diffusional experiment validation of the model.

## 2. Particle characterization

The use of ellipsoids is seen adopted to approximate irregular crushed rocks. (Bagheri *et al.*, 2015) study found that particle size and shape characterization is important in the understanding of packed beds with irregular shapes like rocks. The paper recommends the approximation of the volume of the irregular shape to the volume equivalent ellipsoidal diameter. The equivalent diameter $d_p$ defined as

$$d_p = \sqrt[3]{6V_p/\pi} \tag{1}$$

The particles used in the study consist of concrete moulded in the shape of ellipsoidal particles with equivalent diameter of crushed rocks of $0.0571m$. The particles were randomly selected, and the particles cast are of equal shape and size mimicking the physical rock properties. The particles were cast/pressed using a one-to-one ratio of cement to sand respectively and these are available at the Mechanical Engineering heat transfer lab, Stellenbosch University.

**Figure 1. Illustration of dimension of Ellipsoid**

The volume $V_p$ and the surface are of the ellipsoid as stated by ("Elements of Geometry - Numericana", n.d.) states that below where $A, B, C$ are radii of long, intermediate, and short axes of the particle respectively. An illustration of a cross section of the ellipsoid is as shown in Figure 2. The ellipsoid particle dimensions were 88mm by 59mm by 38mm therefore A = 44mm, B = 29.5mm and C = 19mm

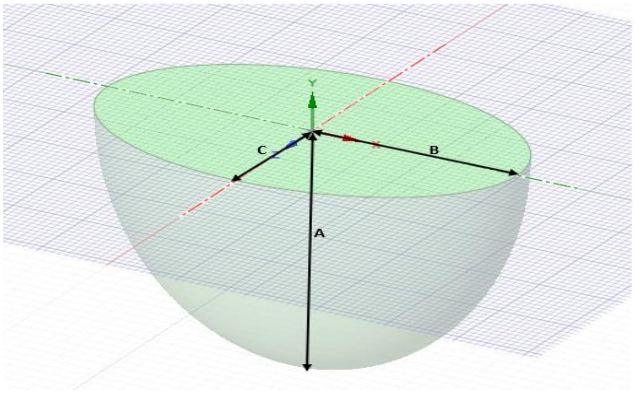


**Figure 2. Illustration of cross section dimension of Ellipsoid**

Particles samples were weighed to obtain 0.23kg, and their volume was calculated using the equation 2 and a volume of the individual particle determined is $1.03304\times 10^{-4} m^3$. The same equation helped to calculate particle density and it was found to be $2{,}226.52\ kg/m^3$. The accuracy of equation 3 approximates the surface area of the particles within about 1% of the actual value.

$$V_p = \frac{4\pi}{3} ABC \tag{2}$$

$$SA \approx 4\pi \left[ \frac{(AB/4)^{8/5} + (AC/4)^{8/5} + (BC/4)^{8/5}}{3} \right]^{5/8} \tag{3}$$

## 2.1. Porosity

(Zavattoni et al., 2011) defines porosity of packed bed as the ratio of the void volume $V_v$ with respect to the total bed volume $V_t$ simplified as

$$\varepsilon = \frac{V_v}{V_t}$$

Henceforth that means that the void volume is approximated to the volume of the boundary filled with the particles minus the total volume of the particles $V_p$ of known number of particles N. Therefore, porosity larger number of particles can be defined as

$$\varepsilon = \frac{V_t - NV_p}{V_t} \tag{4}$$

$$\varepsilon = 1 - \frac{NV_p}{V_t} \tag{5}$$

The most common experimental determination of porosity is water displacement and has been adopted in various literature. (Benyahia, 2005) adopted water displacement to determine the mean voidage of packed beds of polydisperse particles. The routine of water displacement required care and consistency to maintain the accuracy of the data, and the use of the method was limited due to the different shapes of the particles. Since the particles in use are of a similar volume, the use of equation (5) is adopted through an experimental method of individually counting the particles into a container of known volume till the container is full. The experiment is repeated over 5 different runs and an average porosity of 0.428 is obtained.

## 2.2. Angle of repose

The physical quantity of the angle of repose can be defined the cone angle made by a material, with respect to the horizontal when piled (Ileleji and Zhou, 2008). The angle of repose is relevant as it's an essential parameter in understanding granular behaviour(Beakawi Al-Hashemi and Baghabra Al-Amoudi, 2018).

There are different types of angles of repose which include static and dynamic whose description is associated with specific behaviour and application. (Horn, 2012) describes the different methodologies to determine the angle of repose parameter and this paper adopted the static angle of repose methodology and experimental procedure to determine the angle of repose. The ease of experimental interpretation of the results is important though the entire understanding of angle of repose to many researchers challenging. The use of the method depends on the physical property of the material used, such as particle shape and the friction between the individual particles.

### 2.1.1 Experimental procedure

We determined the angle of repose by dropping the individual particle into a container of a diameter of 345mm till the container is full. The container was selected since it can accommodate up to six particles of equivalent diameter of 57.1mm across the selected container is six particles.

When the container is filled, the container is turned upside down and then slowly lifted allowing the material to flow out freely under gravity forming pile of ellipsoids. Using a digital protractor, the instrument is placed along the hypotenuse of the pile of ellipsoids, the angle is measured. The experiments are repeated four times and the average angle of 43.5° is determined as shown in table 1.


**Figure 3. Illustration of determination of angle of repose**

**Table 1: Summary of the experimental angles of repose obtained**

| Parameter | Test 1 | Test 2 | Test 3 | Test 4 | Average |
|---|---|---|---|---|---|
| **Angle of Repose/°** | 45 | 41 | 40 | 48 | 43.5 |

The angle of repose had significant effect on the interparticle properties static friction while investigating the effects of particle properties on angle of repose and flow rate on the particle physical properties of Young's modulus, friction parameters and coefficient of restitution (Yan *et al.*, 2015).

The determination of static and dynamic friction experimental is cumbersome and expensive as it needs special equipment, while the use of software such as DEM could save resources.

DEM uses a numerical methodology to understand individual granular particle-to-particle interactions, and particle-boundary interactions which are under the influence of gravity (Fonte, Oliveira and Almeida, 2015). The commercial Rocky-DEM was used in this study.

### 2.3. DEM Calibration

(Horn, 2012) calibrated the DEM using input parameters of the particles adjusting bulk density, porosity, Young's Modulus, and the angle of repose. He suggested that the angle of repose could be within 1-3% of the measured values. It is important to have defined input parameters that are correct and backed by literature or experiments to ensure accurate modelling of particles properties in the DEM.

The angle of repose tests provides a method to calibrate the DEM model against experimental measurements of angle of repose described in section 2.1.1. The DEM software comes with default frictional coefficients which are adjustable to match the particle property.

With a similar approach as described in section 2.1.1, the angle of repose experiment experimental procedure is replicated in the RockyDEM. The particle imported into the DEM had similar properties in section 2. The particles drawn using CAD software were imported into the DEM consisting of a custom geometry of a container with similar dimensions as in experiment. This helps to eliminate errors and maintain consistency between the experiment and the numerical method.

After the container is full and levelled, a motion frame is introduced onto the container moving upwards in the y-direction with a velocity of 1 m/s to replicate a slow removal of the container as in the experiment and the simulation depicts a similar situation as the experiment as shown in Figure 3. The angle of repose is determined at the default static of the DEM.
The angle of repose was then obtained by means of approximation visual inspection copied into space claim. The final front and side views of the pile were used as in Figure 4, after which the average of the three to four readings were taken as the numerical angle of repose.

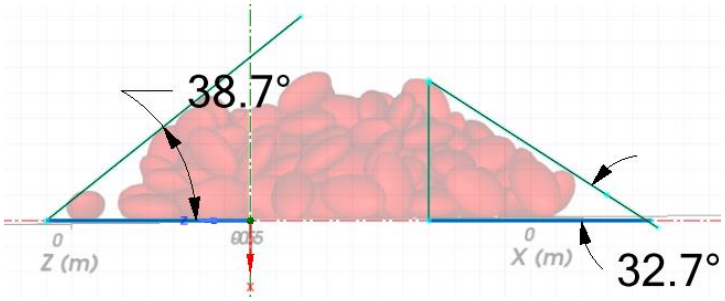


**Figure 4. Default static friction visual inspection of the angle of repose**

The static friction coefficient is adjusted at a 4% increase from the default static coefficient of 0.7 until the predicted and experimentally observed angle of repose is matched keeping the particle properties and other DEM properties at their defaults. This is done to minimise the variation between the experiment and the numerical method using equation 6

$$Error = \frac{Experimental - Simulation\ data}{Experimental} \times 100 \qquad (6)$$

**Table 2: Calibration of static friction against angle of repose**

| Parameter | Default | +4% | +8% | +12% | +16% | +20% |
|---|---|---|---|---|---|---|
| **Static Friction** | 0.7 | 0.728 | 0.756 | 0.784 | 0.812 | 0.84 |
| **Angle of Repose** | 35.9 | 37.2 | 36.4 | 38.6 | 42.475 | 43 |
| **Error/%** | 17.47 | 14.48 | 16.32 | 11.19 | 2.36 | 1.15 |

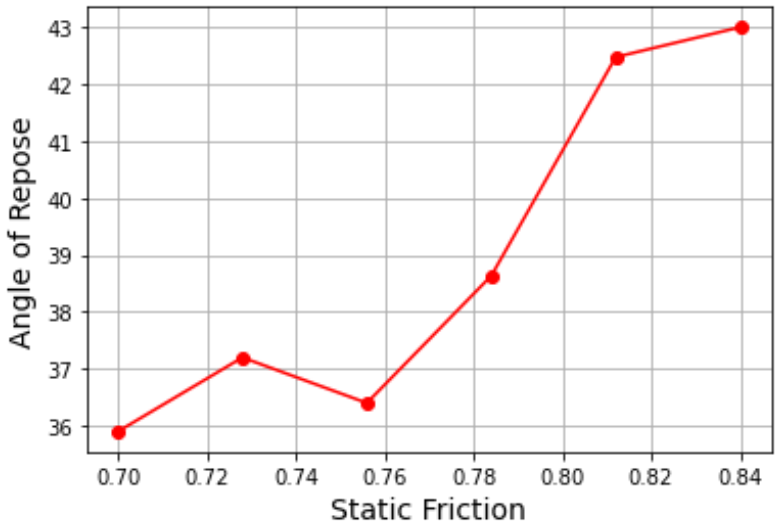


**Figure 5. Angle of repose verse static friction**

## 3. Research methodology

### 3.1. DEM Implementation

The DEM allows the interaction of individual particles, and the movement of these particles are continuously traced (Coetzee & Nel, 2014). The use of DEM allows individual particles to have individual particle position, orientation, and position. The particle positions depend on the interaction between the adjacent particles or if an external force is aced onto the particle.

(Hoffmann, 2021) DEM generated particles, the energy from the impact of dropping the particles caused particles to be randomly packed.

We created a randomly packed bed of monodispersed particles, by dropping them from 1.5m higher up injecting more kinetic energy into the bed ending up with a more "settled" or close packing in the end.

Ellipsoidal particles with dimensions of 88mm by 59 mm by 38 mm were created and drawn by the CAD Space Claim. The created particle is imported into the commercial DEM code Rocky 4.1. The faceted particle introduced into the Rocky-DEM was adjusted to 200 facets to accommodate for the computational power and time of the simulation. The particle development of the ellipsoid into the DEM underwent a transformation from the real-life particle to a faceted particle

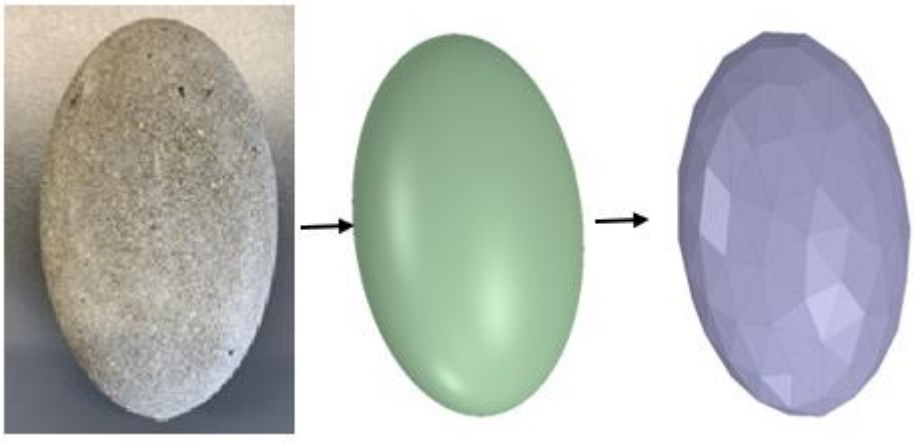

**Figure 6. Transformation of particle from concreted particle to CAD to faceted particle**

Into a custom domain, the particles are released and arrange themselves randomly due to the kinetic energy as they hit the bottom of the geometry.

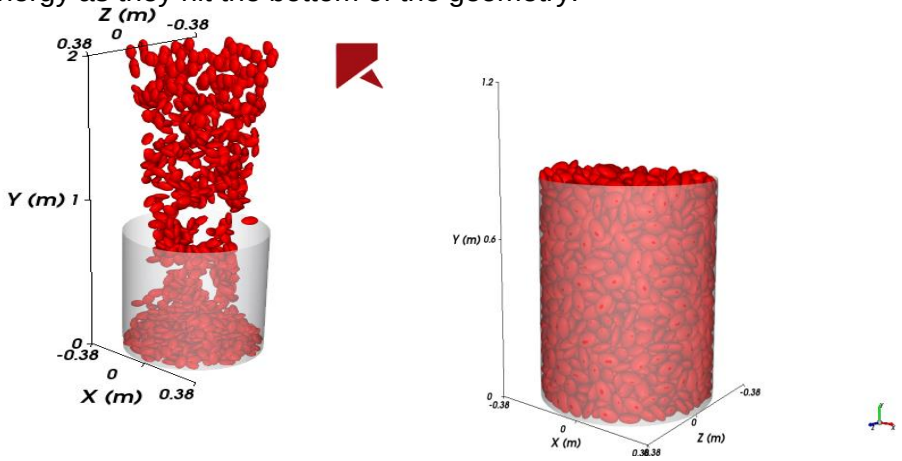


**Figure 7. DEM simulation**

At the end of the DEM simulation, an individual particle position vector is obtained, and the csv file data processing and sorting is done using Microsoft excel. The rotational vectors (the vector around which the particle is rotated), are obtained from the sorted data of the orientation vector by a cross product of orientation vectors in the x, y and z with the position vector of [0,0,1].

The porosity of the DEM is obtained using equation 5 varies by 2.75% very close to the experiment porosity.

### 3.2. Computational fluid dynamics

A master ellipsoidal particle was created in ANSYS Space Claim with its longest axis pointing in the y-direction and its intermediate axis in the x-direction. A Python script is written that reads the cleaned and sorted csv file, the code replicates and copies the master particle and then rotates it by the angle of rotation about the rotation vector, and then translates it to the correct position. The Python script saves time as it automatically replicates the particle using the data processed and sorted from the use of Excel. When all the positions of the particles have been translated, the master ellipsoid was deleted.

In the next step, the generated domains' boundary conditions were defined these included the boundary inlet, outlet, rocks, and walls/tube under no slip condition. The interparticle contact point treatment is important if not the simulation could be difficult and expensive especially for increased number of skewed cells leading to convergence problems and consequently increasing on the computational time (Eppinger, Seidler and Kraume, 2011). The different approach to contact treatment methods includes the gap approach, overlap and bridge. This paper adopted the gap approach where the particle sizes were scaled by 98% reducing the sizes of the particle by 2%. This same method was proposed by (Nijemeisland and Dixon, 2001). The Boolean Operation subtracts was initiated to subtract the particles from the tube to obtain the interstitial flow domain only and the interstitial volumes inside the rock particles.

#### 3.2.1. Meshing

The mesh was created using the ANSYS Workbench Fluent Mesher. Generating a proper mesh is important during the simulation in CFD as the quality of the mesh and size influence on the accuracy and convergence of the solution. The lower the quality of the mesh leads to inaccuracies of the simulation solution whilst high-quality resolutions result in command of higher computational requirements. The mesh independence study was conducted by determining tortuosity at different volume mesh size of 0.04m, 0.038m, 0.048m and 0.056m. This resulted in the change of cell count. All simulations were conducted at constant velocity of 0.01m/s and at the end of the iterations, local tortuosity extracted.

The study adopted a polyhedral mesh, with a maximum cell size of 0.2m, the cell-to-cell growth rate of 1.2 with a minimum cell size of 0.0002mm and a total cell count was 3,543,209. The mesh size used was fine and it had no impact on the computational cost except for more time for convergency of the solution. The mesh is shown in Figure 8. The rocks region was finely meshed as there will be a possibility of large velocity gradients within the interstitial volume regions.

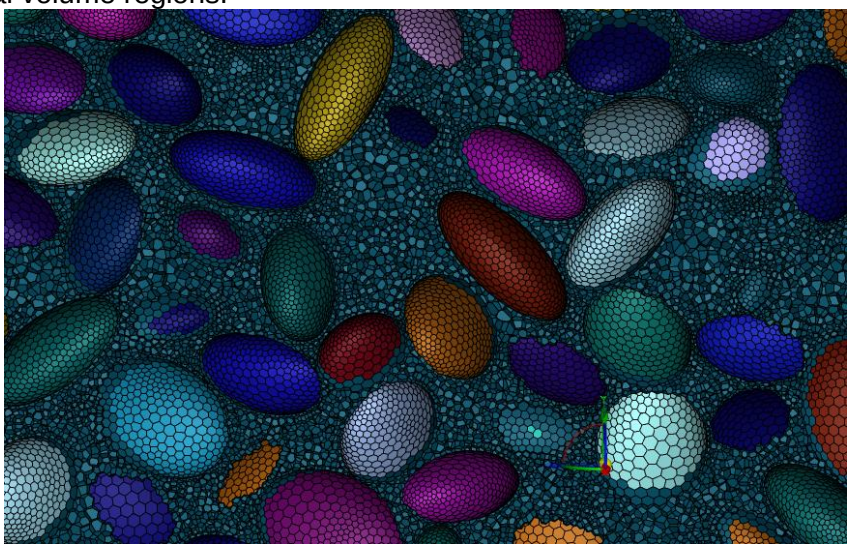

**Figure 8. Mesh Domain**

### 3.2.2. Viscous modelling

The study adopted the laminar model for the investigation of flow through the bed using the Fluent. A constant velocity inlet at the flow inlet assumption of air being incompressible. Pressure-velocity coupling helps solve the fluid flow simulation using a SIMPLE pressure-velocity algorithm. The second order upwind spatial discretisation was selected for all the simulations. The simulations were terminated when the pressure drop across the bed converged to a constant value and the residual scaled plots remained constant. Different simulations were done using different inlet velocities of 0.01, 0.02, 0.03, 0.04, 0.08 and 0.1m/s. at the end of convergence and another simulation is started again with a different velocity

### 3.2.3. Generating path lines

The inbuilt post-processing tool in Ansys Fluent helps generate and build path lines that depend on individual particle velocity vectors which help in the tracing of individual paths across the domain of crushed rocks.

A Python code was developed that calculates the distance between two points in space which states that the distance between two points in $xyz$-space is the square root of the sum of the squares of the differences between corresponding coordinates. That is, given $P_1 = (X_1,\ Y_1,\ Z_1)$ and $P_2 = (X_2,\ Y_2,\ Z_2)$, the distance between $P_1$ and $P_2$ is shown as in equation 7

$$Distance(P_1, P_2) = \sqrt{(X_2 - X_1)^2 + (Y_2 - Y_1)^2 + (Z_2 - Z_1)^2} \tag{7}$$

The python code uses the data from the excel. The code works by locating the already clean excel sheet, and then it indexes sheets by column with locating the first column named as x-coordinate, checking for float, strings, and integers, and appending each individual path lines' x-coordinate. This is repeated for the y, and z coordinates and each coordinate position final values appended are determine. The code then uses NumPy to determine the total length of each path line using equation 7 and the lengths of all the path lines are averaged.

### 3.2.4. Volume integrals technique

Volumetric integral computes the total sums of the product of the cell volume and the selected field variable. (Duda, Koza and Matyka, 2011) used velocity geometries to understand fluid velocity field, without the need of determining streamlines expressing tortuosity was expressed of volumetric integral

$$\tau = \frac{\langle v_{mag} \rangle}{\langle v_x \rangle} \tag{8}$$

ANSYS deploys this tool in post processing to quickly calculated and calibrate field variables in a selected cell zone and the results calculated in the console. The console allows communication and interaction with the user displaying information. With post processing, the console was used to display tortuosity using equation 8 to display calculated variables.

**Table 3: Console calibrated tortuosity**

| Velocity m/s | Tortuosity |
|---|---|
| 0.01 | 1.102 |
| 0.02 | 1.112 |
| 0.04 | 1.115 |
| 0.08 | 1.118 |
| 0.1 | 1.115 |

### 3.3. Diffusion Experiment

The movement of gases takes place from places of higher concentration to regions of lower concentration till when an equilibrium is reached within the system. Diffusion is the net movement of molecules of gases and mathematical theory of diffusion based on how diffusion causes the concentration to change with respect to time(Crank, 1975).

$$\frac{\partial C}{\partial t} = D_{eff} \frac{\partial^2 C}{\partial^2 x} \tag{9}$$

where $D_{eff}$ is the effective molecular diffusion coefficient, C the gas concentration of diffusing particle, x the distance along to the section.

Different methodologies have been used to determine effective coefficient of diffusion and there have been many attempts to find a unique relationship between effective diffusion coefficient to the diffusion coefficient in free air and the porosity(Wardani *et al.*, 1960). The pore structure typically takes up the shape and the porosity of the porous media. Therefore, the effective diffusion accounts for the effect of physical properties including tortuosity and pore size (Thorbjørn *et al.*, 2008). Understanding effective molecular diffusion coefficient is associated with particle movement and the type of porous media the particles are diffusing through.

### 3.3.1. Experiment

The experimental setup consists of a cylindrical container containing ellipsoid particles with one end having a funnel-hood with a 25mm diameter hole and on the other end is a stainless-steel diamond wire mesh raised expanded metal. Three RS PRO RS GD-38 Combustible Gas Leak Detectors were used to determine the concentration of hydrogen at three different positions. A gas pipe feeds hydrogen to the test section from the pressure regulator mounted on a 1.17 kg of compressed hydrogen gas cylinder. The rest of the equipment include, thermocouples, a data logger, and a stopwatch.

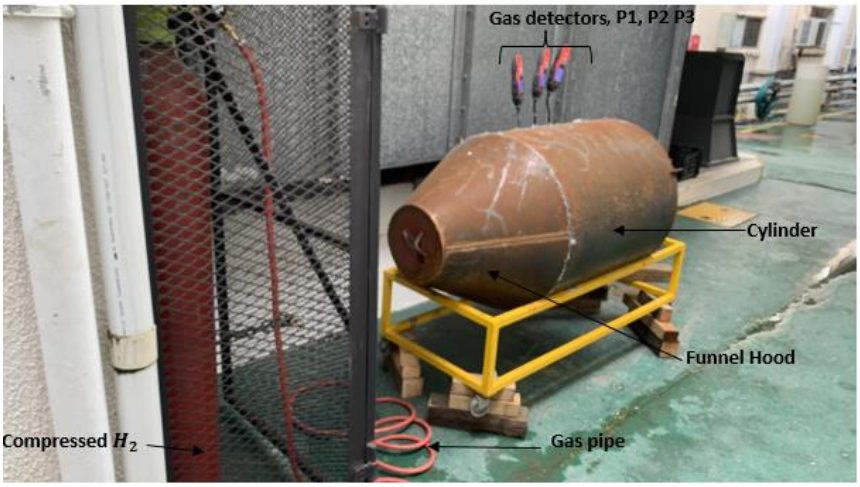


**Figure 9. Visualization of experiment**

The cylinder was filled with cemented ellipsoid that were randomly collected and loaded into the cylinder, with gas sensors inserted into the container to measure gas concentration as shown in figure 9. The gas pipe is then hydrogen gas is injected into the funnel-hood space. The gas pipe is then removed, and the hole is sealed. The concentration of the gas is measured at three different positions of P1, P2 and P3 at a frequency of measurement after every 10 minutes with an initial reading of the concentration taken inside the funnel hood. The experiment is continued for 1 hour and 40 minutes.

Due to diffusion, the concentration of the gas over time continually drops and the sensitivity of the gas detectors readjusted to Low sensitivity.

#### 3.3.1.1. Estimation of Diffusion coefficient

If we assume and consider the cylinder as one-dimensional diffusion flow, therefore concentration of the hydrogen gas diffusing through the packing of ellipsoids is then a function of the length occupied by the ellipsoids and time taken for the diffusing particles of the hydrogen gas. During the injection of the gas, the initial gas concentration $C_0$ is recorded using the gas sensors. Assuming that atmospheric concentration of the hydrogen is zero as in equation

$$C(x > 0\ ,0) = 0 \tag{10}$$

The diffusion experiment's initial and Dirichlet boundary conditions as stated below

$$C(x <\ ,0) = C_0 \tag{11}$$

$$C(0,t) = 0 \tag{12}$$

$$\frac{\partial}{\partial x} C(l,t) = 0 \tag{13}$$

$$\lim_{t\to\infty} C(x,t) = 0 \tag{14}$$

The solution of the equation 9 with boundary conditions 10-14 through the use of separation of variables and imposition of the boundary conditions to propagate into a general solution 15

$$C(x,t) = \sum_{k=1}^{\infty} sin\left(\frac{k\pi}{2L}x\right)\left(\frac{2}{L}\int_0^L C_0\, sin\left(\frac{k\pi}{2L}x\right)dx\right) exp\left[-D_{eff}\left(\frac{k\pi}{2L}\right)^2 t\right] \tag{15}$$

## 4. Results

### 4.1. Estimation of effective diffusion coefficient

To estimate the effective diffusion coefficient of hydrogen through the concrete ellipsoid particles, using the partial differential equation (PDE) 15. The PDE was fit to the measured concentration measured using the gas sensors at positions P1, P2 and P3 that is to say 0.213m, 0.3196m and 0.426m respectively. Each observed concentration at each point was used to fit equation 15 and statistically using the R-squared coefficient of determination to fit the PDE onto the experimental concentration results while optimizing for a unique $D_{eff}$.
The R-squared ($R^2$) helped determine the quality of the model fit against the experiment results. The PDE model and the experimental results were analysed using Excel Microsoft and the infinite sum of the modelled PDE was summed using the first 10 terms. As expected, the concentration of the gas gradually decreases with time as shown below.
The fit displays a good agreement with the experimental data with $R^2$ of 0.8 and greater with the diffusion of coefficient of $4.5 \times 10^{-5} m^2/s$. This suggests significant agreement of the PDE model with the experimental results.

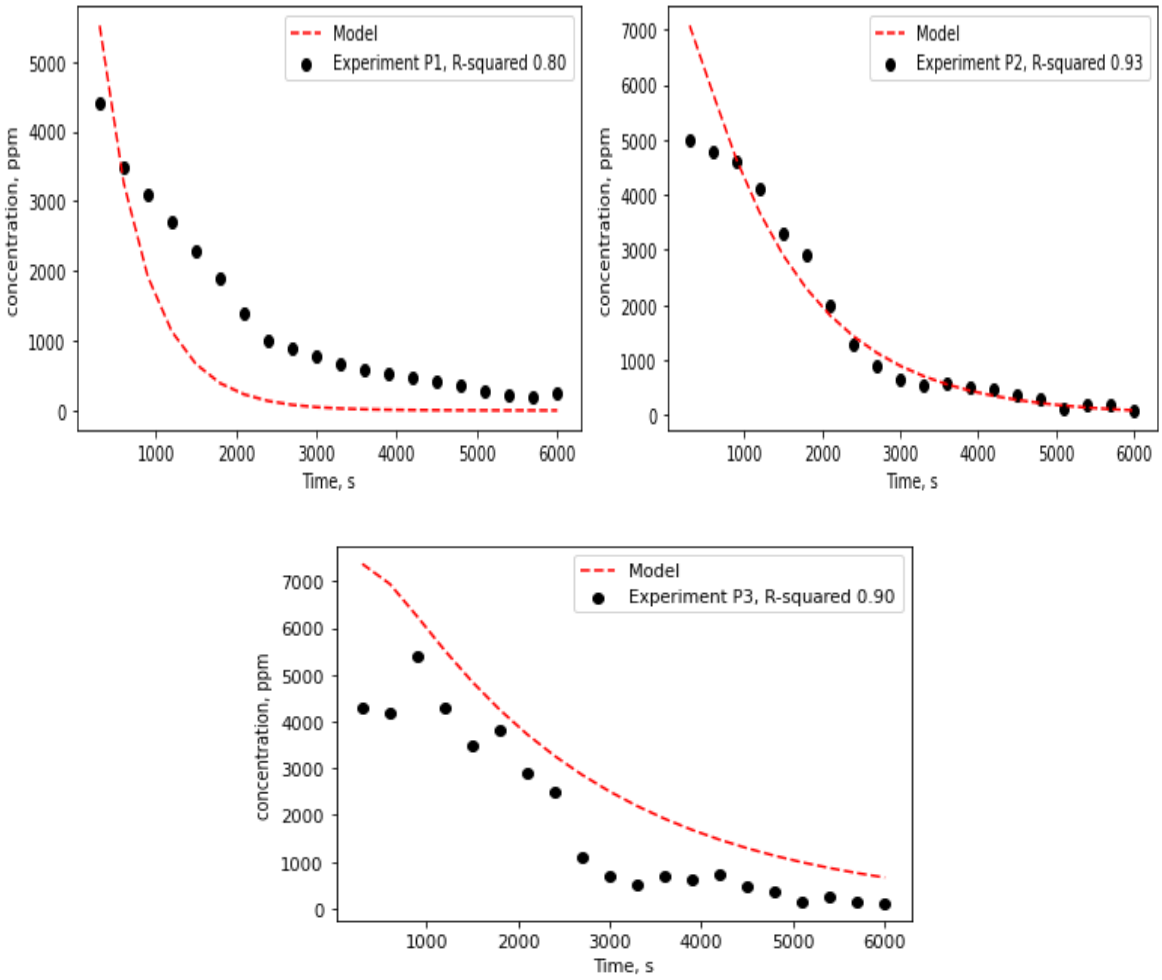


**Figure 10. Graphs of fitted PDE on experimental data at points P1, P2 and p3**

The experiments were primarily carried out to understand the net movement of hydrogen gas through a porous media containing ellipsoid rocks. The use of effective diffusion coefficient to estimate tortuosity has been presented by (Delgado, 2006).

### 4.2. CFD/DEM model validation

A maximum deviation of 10.56% and an average deviation of 6.79% were obtained between the path line and volumetric methods of determination of tortuosity, with a slight average of 14% for the path line technique to the diffusion methodology. This stipulates that the method of volumetric integral method to determine tortuosity does not deviate far and is very close approximation to the path line technique. The only attributes to the changes are limited to velocity variations which provides uncertain drastic change in the estimated tortuosity parameter.

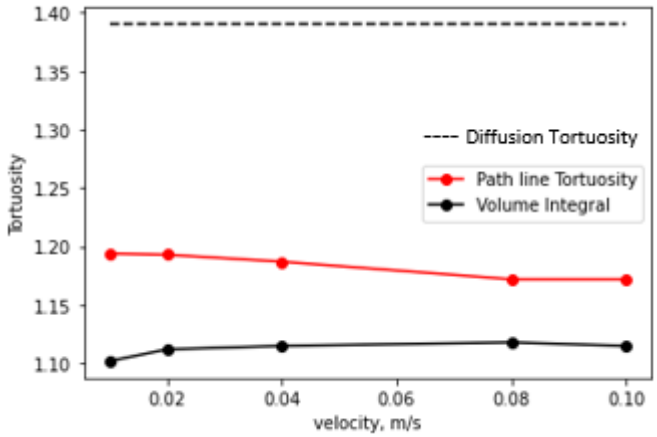


**Figure 11. Tortuosity of the diffusion, path line and volume integral**

The deviation with the experiment could be attributed to the facility set up and the behaviour of hydrogen gas and its physical properties and the limitations of having airtight container though we tried to control the surrounding conditions as far as possible. Although the diffusion coefficient in P1 was smaller than the corresponding P2 and P3, this was attributed to P1 being closer to the injection point. All concentration modelled data highly correlated with R-squared greater than 0.8 providing higher confidence in the modelled $4.5 \times 10^{-5} m^2/s$. The concentration data highly determine the fit of the model and help in determination of diffusion coefficient which highly depend on factors that influence diffusion of gases.

## 5. Conclusions and recommendations

Calibration of the DEM was conducted to investigate the correlation between angle of repose and static friction, and to create a model resemblance to real life packed bed of concrete ellipsoids. The generated DEM bed was of higher level of significance with very close correlation to the physical bed with a porosity less than 2.75%, and the angle of repose within 1.15% of the experimental values. In this paper, we used a DEM to generate randomly packed beds of ellipsoidal particles, and CFD to simulate the path lines through the particles at constant velocity. The path lines enabled to generate of tortuosity. The simulation's path line tortuosity was validated against diffusion experiments using hydrogen with ellipsoidal particles. The paper investigates the deviation noticed as path lines move through particles, and this deviation is caused by a tortuosity tensor. Foresaid, this investigation was to improve on the deviation noticed in a simulation of crushed rocks (Hoffmann, 2021) by introducing tortuosity to the coefficient of resistance tensors to improve on the viscous and inertial resistance tensors.

## References

Allen, K.G. *et al.* (2014) 'Rock bed storage for solar thermal power plants: Rock characteristics, suitability, and availability', *Solar Energy Materials and Solar Cells*, 126, pp. 170–183. Available at: https://doi.org/10.1016/j.solmat.2014.03.030.

Allen, K.G. (2014) *Rock bed thermal storage for concentrating solar power plants*. Available at: http://scholar.sun.ac.za.

Allen, K.G., von Backström, T.W. and Kröger, D.G. (2013) 'Packed bed pressure drop dependence on particle shape, size distribution, packing arrangement and roughness', *Powder technology*, 246, pp. 590–600. Available at: https://doi.org/10.1016/j.powtec.2013.06.022.
Allen, K.G., von Backström, T.W. and Kröger, D.G. (2014) 'Packed rock bed thermal storage in power plants: Design considerations', in *Energy Procedia*. Elsevier Ltd, pp. 666–675. Available at: https://doi.org/10.1016/j.egypro.2014.03.072.
Bagheri, G.H. *et al.* (2015) 'On the characterization of size and shape of irregular particles', *Powder Technology*, 270(Part A), pp. 141–153. Available at: https://doi.org/10.1016/J.POWTEC.2014.10.015.
Beakawi Al-Hashemi, H.M. and Baghabra Al-Amoudi, O.S. (2018) 'A review on the angle of repose of granular materials', *Powder Technology*, 330, pp. 397–417. Available at: https://doi.org/10.1016/J.POWTEC.2018.02.003.
Benyahia, F. (2005) 'Enhanced Voidage Correlations for Packed Beds of Various Particle Shapes and Sizes', *Particulate Science and Technology*, 23(2), pp. 169–177. Available at: https://doi.org/10.1080/02726350590922242.
Carman P (1937) 'Fluid flow through granular beds', *Trans. Inst. Chem. Eng.*, 15, pp. 150–166.
Coetzee, C.J. and Nel, R.G. (2014) 'Calibration of discrete element properties and the modelling of packed rock beds', *Powder Technology*, 264, pp. 332–342. Available at: https://doi.org/10.1016/j.powtec.2014.05.063.
Crank, John. (1975) *The mathematics of diffusion*. Clarendon Press.
Delgado, J.M.P.Q. (2006) 'A Simple Experimental Technique to Measure Tortuosity in Packed Beds', *The Canadian Journal of Chemical Engineering*, 84(6), pp. 651–655. Available at: https://doi.org/10.1002/CJCE.5450840603.
Duda, A., Koza, Z. and Matyka, M. (2011) 'Hydraulic tortuosity in arbitrary porous media flow', *Physical Review E - Statistical, Nonlinear, and Soft Matter Physics*, 84(3). Available at: https://doi.org/10.1103/PhysRevE.84.036319.
*Elements of Geometry - Numericana* (no date). Available at: http://www.numericana.com/answer/geometry.htm#ovalsolid (Accessed: 8 June 2022).
Eppinger, T., Seidler, K. and Kraume, M. (2011) 'DEM-CFD simulations of fixed bed reactors with small tube to particle diameter ratios', *Chemical Engineering Journal*, 166(1), pp. 324–331. Available at: https://doi.org/10.1016/J.CEJ.2010.10.053.
Fluri, T.P. (2009) 'The potential of concentrating solar power in South Africa', *Energy Policy*, 37(12). Available at: https://doi.org/10.1016/j.enpol.2009.07.017.
Fonte, C.B., Oliveira, J.A.A. and Almeida, L.C. de (2015) 'DEM-CFD COUPLING: MATHEMATICAL MODELLING AND CASE STUDIES USING ROCKY-DEM® AND ANSYS FLUENT®'.
Garrouch, A.A., Ali, L. and Qasem, F. (2001) 'Using Diffusion and Electrical Measurements to Assess Tortuosity of Porous Media', *Industrial & Engineering Chemistry Research*, 40(20), pp. 4363–4369. Available at: https://doi.org/10.1021/ie010070u.
Ghanbarian, B. *et al.* (2013) 'Tortuosity in Porous Media: A Critical Review', *Soil Science Society of America Journal*, 77(5). Available at: https://doi.org/10.2136/sssaj2012.0435.
Hoffmann, J. (2021) 'A CFD/DEM Approach to Determine the Flow Resistance of Randomly Packed Bed of Crushed Rock Particles', (140). Available at: https://doi.org/10.11159/ffhmt21.140.
Hoffmann, J.E. (2018) 'Pressure drop though random and structured beds of ellipsoidal particles', 2033, p. 80021. Available at: https://doi.org/10.1063/1.5067108.
Hölzer, A. and Sommerfeld, M. (2008) 'New simple correlation formula for the drag coefficient of non-spherical particles', *Powder Technology*, 184(3), pp. 361–365. Available at: https://doi.org/10.1016/J.POWTEC.2007.08.021.
Horn, E. (2012) *The calibration of material properties for use in discrete element models*.
Ileleji, K.E. and Zhou, B. (2008) 'The angle of repose of bulk corn stover particles', *Powder Technology*, 187(2), pp. 110–118. Available at: https://doi.org/10.1016/J.POWTEC.2008.01.029.

Kozeny, J. (1927) ‘Uber kapillare leitung der wasser in boden’, *Royal Academy of Science, Vienna, Proc. Class I*, 136, pp. 271–306.
Nijemeisland, M. and Dixon, A.G. (2001) ‘Comparison of CFD simulations to experiment for convective heat transfer in a gas–solid fixed bed’, *Chemical Engineering Journal*, 82(1–3), pp. 231–246. Available at: https://doi.org/10.1016/S1385-8947(00)00360-0.
du Plessis, J.P. and Woudberg, S. (2008a) ‘Pore-scale derivation of the Ergun equation to enhance its adaptability and generalization’, *Chemical Engineering Science*, 63(9), pp. 2576–2586. Available at: https://doi.org/10.1016/J.CES.2008.02.017.
du Plessis, J.P. and Woudberg, S. (2008b) ‘Pore-scale derivation of the Ergun equation to enhance its adaptability and generalization’, *Chemical engineering science*, 63(9), pp. 2576–2586. Available at: https://doi.org/10.1016/j.ces.2008.02.017.
Sun, Z., Tang, X. and Cheng, G. (2013) ‘Numerical simulation for tortuosity of porous media’, *Microporous and Mesoporous Materials*, 173. Available at: https://doi.org/10.1016/j.micromeso.2013.01.035.
Thorbjørn, A. *et al.* (2008) ‘A Gas Diffusivity Model Based on Air-, Solid-, and Water-Phase Resistance in Variably Saturated Soil’, *Vadose Zone Journal*, 7(4), pp. 1276–1286. Available at: https://doi.org/10.2136/vzj2008.0023.
Wardani, D.K. *et al.* (1960) ‘Gaseous diffusion in porous media. Part 2. - Dry granular materials’, *British Journal of Applied Physics To*, 11, p. 318.
Yan, Z. *et al.* (2015) ‘Discrete element modelling (DEM) input parameters: understanding their impact on model predictions using statistical analysis’, *Computational Particle Mechanics*, 2(3), pp. 283–299. Available at: https://doi.org/10.1007/S40571-015-0056-5/TABLES/6.